Open access • Journal Article • DOI:10.1016/J.JQSRT.2005.05.053

Purgatorio—a new implementation of the Inferno algorithm — Source link

Brian G. Wilson, V. Sonnad, P. A. Sterne, W. Isaacs

Institutions: Lawrence Livermore National Laboratory

Published on: 01 May 2006 - Journal of Quantitative Spectroscopy & Radiative Transfer (Pergamon)

LAWRENCE
LIVERMORE
NATIONAL
LABORATORY

UCRL-JRNL-211007

Purgatorio - A new implementation of the Inferno algorithm

B. Wilson, V. Sonnad, P. Sterne, W. Isaacs

April 1, 2005

Journal of Quantitative Spectroscopy and Radiative Transmission

Purgatorio – A new implementation of the Inferno algorithm

B. Wilson[κ], V. Sonnad, P. Sterne, W. Isaacs

Lawrence Livermore National Laboratory
P.O. Box 808
Livermore, CA 94550

Abstract

An overview of PURGATORIO, a new implementation of the INFERNO[1] equation of state model, is presented. The new algorithm emphasizes a novel decimation scheme for automatically resolving the structure of the continuum density of states, circumventing limitations of the pseudo-R matrix algorithm previously utilized.

1. Introduction

For astrophysical applications, as well as modeling laser-produced plasmas, there is a continual need for equation-of-state data over a wide domain of physical conditions. This paper presents algorithmic aspects for computing the Helmholtz free energy of plasma electrons for temperatures spanning from a few Kelvin to several KeV, and densities ranging from essentially isolated ion conditions to such large compressions that most bound orbitals become delocalized. The objective is high precision results in order to compute pressure and other thermodynamic quantities by numerical differentiation. This approach has the advantage that internal thermodynamic self-consistency is ensured, regardless of the specific physical model, but at the cost of very stringent numerical tolerances for each operation. The computational aspects we address in this paper are faced by any model that relies on input from the quantum mechanical spectrum of a spherically symmetric Hamiltonian operator. The particular physical model we employ is that of INFERNO; of a spherically averaged ion embedded in jellium.

2. Theory

All self-consistent fields rely on the electron charge density

$$\rho(r) = \rho_{bound}(r) + \rho_{free}(r)$$

[κ] Corresponding author. Tel.: 925-423-4636; Fax.: 925-423-7228
E-mail address: wilson9@llnl.gov

$$4\pi r^2 \rho_{bound}(r) \equiv \sum_i f(\varepsilon_i,\mu) 2|\kappa_i| \{P_i^2(r) + Q_i^2(r)\} \qquad 4\pi r^2 \rho_{continuum}(r) \equiv \int_0^\infty d\varepsilon\, f(\varepsilon,\mu) \sum_\kappa 2|\kappa| \{P_{\kappa\varepsilon}^2(r) + Q_{\kappa\varepsilon}^2(r)\}$$

For atomic structure theories using Local-Density-Functional approximations for exchange and correlation the dependence is solely on ρ, in general it enters at least through the classical electrostatic (or Hartree) field. The sign and phase conditions of the major and minor components of the radial Dirac equation for each spin-angular momentum channel κ are outlined in appendix A[2]. Using an ion-sphere or Neutral Pseudo-atom approximation, the potential vanishes outside some radius 'R_{ion}', and we require the neutrality condition

$$\int_0^{R_{ion}} 4\pi r^2 dr\, \rho(r) = Z$$

which determines the chemical potential μ in the Fermi function $f(\varepsilon,\mu)$[3 4].

The computational overhead for precise calculation of the quantum mechanical continuum charge density arises from three considerations:

- First, propagation of a radial wave solution is an inherently recursive loop (the solution at one point on a discretized radial mesh depends on previously obtained adjacent values). At issue is a means to adequately represent waves on any given radial mesh given the highly oscillatory nature of continuum waves for large enough energy or angular momentum.
- Second, large numbers of partial waves must be summed in order to obtain converged results, in particular for high energies or low densities. This is illustrated by the zero field reference system, which has a constant continuum electron density. The constancy of the continuum density results from the Bessel function identity

  $$\sum_{l=0}^{\infty} (2l+1) j_l^2(pr) = 1$$

  In practice, the partial wave summation must be carried for $l > p R_{ion}$ in order to approximate this identity[5]. An issue here is the stability of the Dirac propagator for large angular momentum, also the machine dynamic range becomes a consideration due to the step like behavior of the solution interior to the centrifugal barrier.
- Third, the outermost integration over energy must be performed on a mesh which ultimately resolves detailed resonant features of the density-of-states like quantity

  $$X(\varepsilon) \equiv \sum_\kappa 2|\kappa| \int_0^{R_{ion}} dr\, \{P_{\kappa\varepsilon}^2(r) + Q_{\kappa\varepsilon}^2(r)\}$$

  The issue here is that because X(ε) is time consuming to compute, and the locations of the structure features are a-priori unknown. An *efficient* quadrature scheme, that automatically refines the energy grid in areas as needed, is required.

Because of the computational burden of quantum mechanical calculations many models have relied in the past on the Thomas-Fermi approximation. This approximation may be succinctly obtained from the exact expression (re-written here in operator formalism – $S(x)$ denoting the step function giving unity for positive argument)

$$\rho_{continuum}(r) = Trace\left\{\delta(r-\hat{r}) f\left(\hat{h}_{Dirac},\mu\right) S\left(\hat{h}_{Dirac}\right)\right\}$$

by neglecting the non-commutivity of the kinetic and potential energy operators. Using the complete basis of plane wave states to take the trace, one obtains

$$\rho_{continuum}(r) = \frac{1}{\pi^2}\int_{p_0(r)}^{\infty} p^2 dp\; f\left(\varepsilon[p],\mu\right)$$

where

$$p^2 = \varepsilon\left(2+\alpha^2\varepsilon\right) \qquad \varepsilon[p_o(r)] + V(r) = 0$$

The principle defect of this Thomas-Fermi approximation is that bound states, which upon more compressed conditions dissolve into the continuum (see Figure 1), do not re-appear as resonant features in $X(\varepsilon)$ that conserve the total number of electrons inside the ion sphere. As a necessity, unphysical discontinuous changes in the chemical potential, and therefore the equation-of-state, occur. Non-local or other quantum corrections to the Thomas-Fermi description[6] (such as arise from leading corrections to non-commuting operators) may offer small quantitative improvement in $\rho(r)$ but do not address this fundamental deficiency.

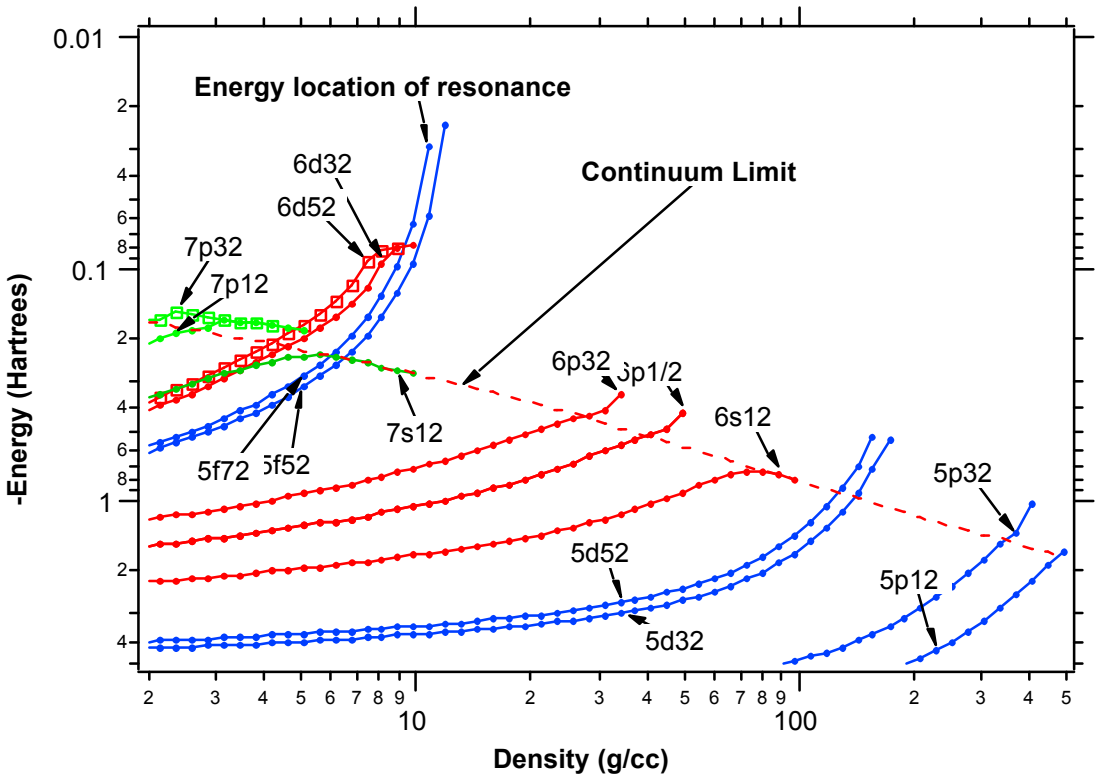

Fig. 1. Eigenvalues for a collection of orbital in a 10 eV Uranium plasma are plotted versus density. The energy axis zero is set by the isolated ion continuum threshold. The dashed line illustrates the lowering of the continuum with density. Below the continuum the curves represent eigenvalues, above, the centroid of a resonant feature when unambiguous. Curves terminate in the continuum region when resonances essentially blend in with the ambient density of states curve. These curves illustrate the typical qualitative behavior of different angular momentum channels. In particular note that S waves do not form resonances.

2. Inferno Approximations

Inferno employs two approximations to calculating the charge density of continuum electrons that greatly reduce the cost of computation.

First, Thomas-Fermi like semi-classical expressions for contributions from high energy and / or high angular momentum channels are grafted on to truncated partial wave decompositions of the exact quantum mechanical formulae. The interested reader should consult the Inferno manual for details[7].

Secondly, all continuum waves are approximated in terms of a small set of basis functions[8]

$$\psi_\varepsilon(r) \cong \sum_i c_i(\varepsilon)\phi_i(r) \qquad \hat{h}_{Dirac}\phi_i = \varepsilon_i\phi_i$$

The form of the interpolation coefficients

$$c_i(\varepsilon) = \sum_j \left(M^{-1}\right)_{ij} \frac{W_{j\varepsilon}}{\varepsilon_j - \varepsilon}$$

reflects the property that the overlap of two continuum waves can be evaluated solely by values at the end of the integration range. For distinct waves

$$(M)_{ab} \equiv \int_0^{R_{ion}} dr\{P_a(r)P_b(r)+Q_a(r)Q_b(r)\}=-\frac{(P_aQ_b-Q_aP_b)\Big|^{R_{ion}}}{\varepsilon_a-\varepsilon_b}\equiv\frac{W_{ab}}{\varepsilon_a-\varepsilon_b}$$

while

$$X\equiv\int_0^R dr\,\{P^2(r)+Q^2(r)\}=\frac{1}{\alpha}\left\{Q\frac{dP}{d\varepsilon}-P\frac{dQ}{d\varepsilon}\right\}\Big|_R$$

The derivations of these identities are presented in Appendix 2. The essential point to note is that the interpolation coefficients depend on the overlap matrix of the basis set, and for low enough density, due to the Kronecker-delta normalization of continuum waves, the matrix becomes ill-behaved. Intuitively; no matter how close in energy one chooses two basis functions, eventually two continuum waves get so out of phase as to be non-interpolative[9]. For this reason Inferno results become unreliable in the low-density limit.

Because of these two approximations results of Inferno do not demonstrate precise *numerical* thermodynamic consistency (See Figure 2)

$$P\overset{?}{\longleftrightarrow}T\left(\frac{\partial P}{\partial T}\right)_V+\rho^2\left(\frac{\partial E}{\partial\rho}\right)_T$$

despite the underlying free-energy functional guaranteeing this property. We have found that checking this consistency provides a very stringent test of numerical procedures.

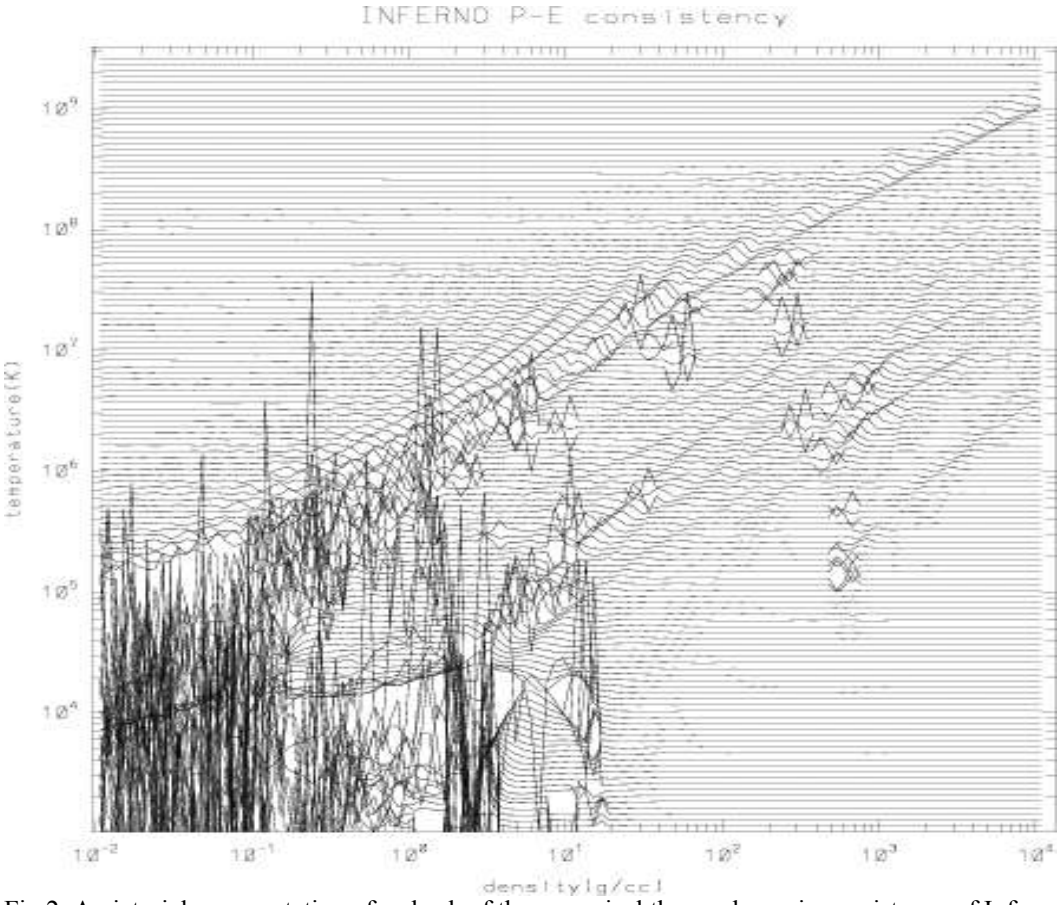

Fig.2 A pictorial representation of a check of the numerical thermodynamic consistency of Inferno. Plotted is pressure "P" divided by $\rho^2 \frac{\partial E}{\partial \rho} + T \frac{\partial P}{\partial T}$ as a function of density for various temperatures. The curves are offset by multiplying the ratio by T. Perfect consistency would result in horizontal curves. Aside from expected difficulties at low densities and temperatures one also sees systematic ripples in part resulting from the grafting of semi-classical approximations.

3. Robust radial wave propagation

The placement of radial grid points is generally determined by requirements imposed for computing bound orbitals in a self consistent field, a dense locus of points is required as near the nucleus. Propagating outward from boundary conditions at the origin, eventually the grid becomes too sparse to adequately resolve continuum wave function oscillations for high energies, or the step like behavior of high angular momentum waves as they are excluded near the origin. The question of wave function representability thus becomes an issue, and necessitated approximations in Inferno. These issues can be circumvented if for the Dirac system of equations

$$\frac{dP}{dr} + \frac{\kappa}{r} P = \{2 + \alpha^2 (\varepsilon - V)\} \tilde{Q}$$

$$\frac{d\tilde{Q}}{dr} - \frac{\kappa}{r}\tilde{Q} = -(\varepsilon - V)P$$

we make the substitutions[10]

$$P(r) = A(r)Sin[\Phi(r)]$$
$$\tilde{Q}(r) = B(r)Sin[\Phi(r)] + \frac{\theta}{A(r)}Cos[\Phi(r)]$$

The resulting system

$$\frac{dA}{dr} = -\frac{\kappa}{r}A + \{2 + \alpha^2(\varepsilon - V)\}B$$
$$\frac{dB}{dr} = \frac{\kappa}{r}B - (\varepsilon - V)A + \frac{\theta^2}{A^3}\{2 + \alpha^2(\varepsilon - V)\}$$
$$\frac{d\Phi}{dr} = \frac{\theta}{A^2}\{2 + \alpha^2(\varepsilon - V)\}$$

are coupled, non-linear, and stiff, but are readily solved with standard solvers. We recommend a Rosenbrock method[11] with analytically evaluated Jacobian, which guarantees a user specified precision by automatic sub-step size adjustment as required. The benefit in using the Phase-Amplitude version[12] of the wave functions lie in their smoothness, allowing for their solution and representation on a much coarser radial grid than would be the case for the usual form[13] [14]. The energy normalization of continuum waves are automatically ensured by the parameter value

$$\theta = \frac{\varepsilon}{p}$$

Note that the phase function is undefined to within a constant – which can be identified with the traditional phase shift. Its value can be determined by propagating the phase-amplitude solution inwards, and then matching onto an outwardly propagated solution generated by traditional (Adams-Moulton) methods where the radial mesh is still adequately dense (See Figure 3).

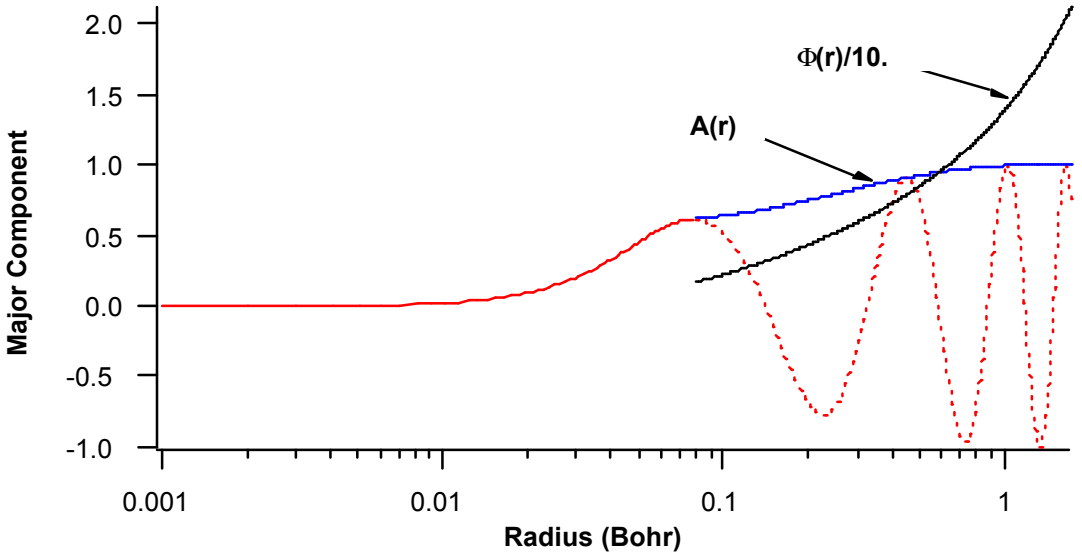

Fig3. A schematic of the hybrid representation of continuum waves. Smooth amplitude and phase functions are propagated inwards from boundary conditions predetermined by normalization conventions. These are matched onto waves propagated outwards by standard methods over domains where the wave is non-oscillatory. The amplitude and phase functions encode the information of the oscillatory nature of the wave (dashed).

4. Automatic energy grid refinement

In order to converge a self-consistent field the chemical potential must be obtained upon integrating X(ε) over energy. By using exact wave-functions at each energy, in lieu of approximant interpolates as does Inferno, each evaluation of X(ε) represents a significant expenditure of computational effort. In the ideal electron gas limit X(ε) behaves approximately[15] as (See Appendix 3)

$$X^{ideal}(\varepsilon) = \frac{1}{\pi^2}\left\{\frac{4}{3}\pi R_{ion}^3\right\} p\left(1+\alpha^2\varepsilon\right) \quad \approx \varepsilon^{1/2}$$

but for an ion embedded in jellium additionally exhibits resonant features (and deficits[16]) about this limit whose position, shape and strength are not easily predicted in advance. (See Figure 4.)

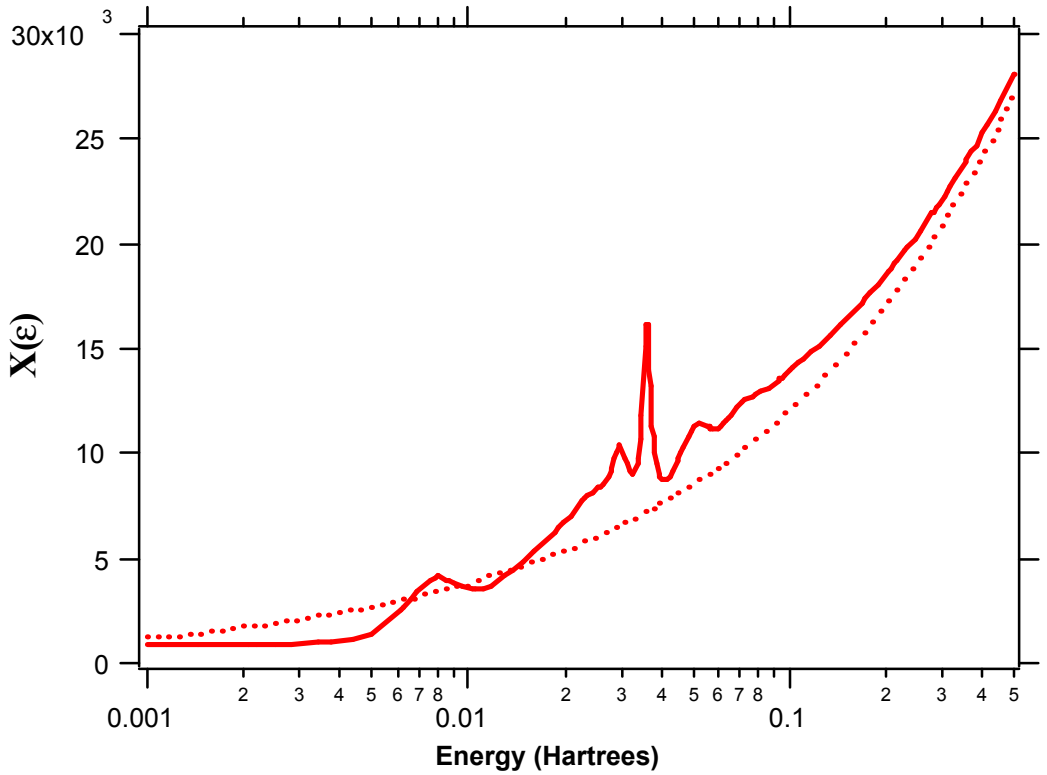

Fig. 4. Continuum charge energy density inside an ion-sphere as a function of density. This quantity is closely related to the continuum density of states. Conditions at U at 10eV and 0.01 g/cc typify general qualitative features – a deficit from the ideal value (dotted line) often seen near the threshold, complex resonant structures, and an asymptotic convergence to ideal wave results at high energies.

The approach we have chosen is to divide the integral

$$\int d\varepsilon\, f(\varepsilon,\mu)X(\varepsilon)$$

into two domains, $\varepsilon=[0,\varepsilon_0]\cup[\,\varepsilon_0,\infty]$. The boundary ε_0 is suitable chosen such past this point $X(\varepsilon)$ is relatively unstructured and the behavior of $f(\varepsilon,\mu)$ is predominantly that of an exponential tail. In that region the integral is computed by some high order ($\approx 90^{th}$) Gauss-Laguerre integration formulae.

The first region is attacked by a common strategy[17]. The finite region is decimated into panels, independent estimates of the quadrature are computed for each panel, and egregiously imprecise panels are continually sub-divided and re-estimated until convergence is acquired. This procedure puts integration points where they are needed most, *automatically* resolving spectral features in $X(\varepsilon)$, and terminates only after a user specified precision in the result is achieved.

A traditional implementation of this scheme would utilize a 4-point Gauss-Legendre formula

$$I \equiv \int_{-h/2}^{+h/2} dx\; f(x) \cong \frac{h}{2}\sum_{i=1}^{4} w_i f(x_i) + Order\left[h^9\right] \qquad x_i = \mp\sqrt{\left(30 \pm \sqrt{480}\right)/70}$$

$$w_i = 1/\left\{15x_i^2\left(1-x_i^2\right)\right\}$$

A second independent estimator for a panel would consist of dividing the panel in half, and applying the above four-point formula to each sub-panel in turn.

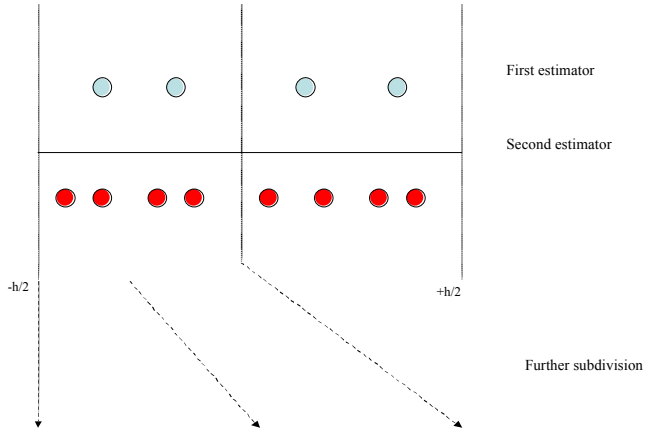

Fig 5. A schematic showing the location of function evaluations for estimating the quadrature in a single panel using traditional Gauss-Legendre formulae. If needed, the panel is subdivided, and each sub-panel in turn plays the role of the parent panel.

The problem with such a scheme, for expensive evaluations of f(x), is that information is not re-used. If the two estimates disagree we have wasted the original four function evaluations and must re-test each sub-interval in turn by further bifurcation. At the level of agreement we have performed eight function evaluations unnecessarily.

In practice it is better to employ few point formulae over more (smaller) panels than higher order formulae over fewer (larger) panels. To improve on efficiency one can consider the second Euler-Maclaurin summation formula

$$\int_{x_1}^{x_N} dx\, f(x) \cong h\{f_{3/2} + f_{5/2} + \ldots f_{N-1/2}\} + \frac{B_2}{4} h^2 (f_n' - f_1') + \ldots$$

Two independent estimators requiring only 3 evaluations per panel would be

$$I^{(a)} = \int_{-h/2}^{+h/2} dx\, f(x) \cong hf(0) + \frac{B_2}{4} h^2 \{f'(h/2) - f'(-h/2)\} +$$

$$I^{(b)} = \int_{-h/2}^{+h/2} dx\, f(x) \cong \frac{h}{3}\left[f(-h/6) + f(0) + f(h/6)\right] + \frac{B_2}{4}\left(\frac{h}{3}\right)^2 \{f'(h/2) - f'(-h/2)\} +$$

however, although the integral is of fourth order in the panel size

$$\int_{-h/2}^{+h/2} dx\, f(x) = \frac{9I^{(b)} - I^{(a)}}{8} + Order\left[h^4\right]$$

the error estimate is only Order[h^2]. Furthermore, sub-division which doesn't waste previous function evaluations requires *tri-furcation* of each panel, and thereby commits us to at least six additional function evaluations.

It turns out that higher order estimates that only bifurcates (so we don't waste evaluations where it is not needed) and optimally re-uses information (to minimize the number of expensive function calls) is unique, but requires asymmetric sub-division. To see this consider the simplest non-trivial (i.e. two-point) panel evaluation

$$\int_{-h/2}^{+h/2} dx\, f(x) \cong w_1 f(x_1) + w_2 f(x_2)$$

If we consider an arbitrary point of sub-division x^* between x_1 and x_2,

$$x^* \equiv -\frac{h}{2} + \Gamma h$$

(Γ is a dimensionless parameter defining the demarcation) then requiring sub-panels to scale self similarly (in order to re-use function evaluations) sets

$$x_1 = x^* - \Gamma\theta h$$
$$x_2 = +\frac{h}{2} - \theta h$$

with θ a second dimensionless free parameter. If we consider Γ as fixed, then we have three variables to make the integration formula exact for the monomials $f(x)=\{1,x,x^2\}$. This results in a non-linear set of equations whose solution is

$$w_1 = \frac{1-2\theta}{(1-\theta)(2-2\Gamma)} \quad w_2 = 1 - w_1$$

where θ satisfies a cubic equation with the roots $\theta=1$ and

$$\theta = \frac{-3 + 9\Gamma \pm \sqrt{3}\sqrt{3 - 10\Gamma + 3\Gamma^2}}{12\Gamma}$$

The constraint that θ be non-negative and less than unity gives the only allowed solution as $\theta=0$ and $\Gamma=1/3$:

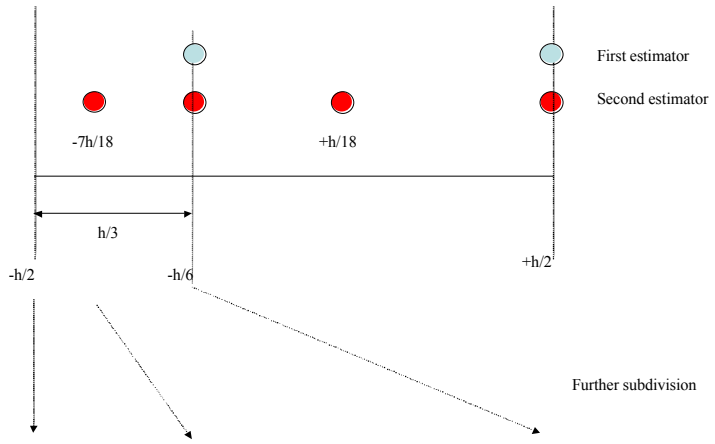

Fig. 6. A schematic showing the location of function evaluations for an embedded quadrature scheme discussed in the text. Panel sub-division asymmetrically splits of a small sub-panel, but re-uses all function evaluations.

We have

$$\int_{-h/2}^{+h/2} dx\, f(x) = \frac{h}{4}\left\{3f\left(-\frac{h}{6}\right)+ f\left(\frac{h}{2}\right)\right\} \quad -\frac{h^4}{36}\frac{f'''(0)}{3!}+ ..$$

The second estimator is formed by adding two evaluation points. Their locations are specified a-priori by self-similar scaling, that is, we place one in each sub-region to play the role that the interior point played in the entire region. Using these locations, but with four new weightings to satisfy exactly the monomials f(x)={1,x,x^2,x^3}, yields

$$\int_{-h/2}^{+h/2} dx\, f(x) = \frac{h}{256}\left\{81f\left(-\frac{14h}{36}\right)- 24f\left(-\frac{h}{6}\right)+162f\left(\frac{h}{18}\right)+ 37f\left(\frac{h}{2}\right)\right\} + Order\left[h^5\right]$$

Note that this second estimator formula may be obtained by using the first estimator formula for the original and each of the two sub-panels intervals

$$I^{(0)} \equiv \int_{-h/2}^{+h/2} dx\, f(x) = I^{(a)} + I^{(b)} \equiv \int_{-h/2}^{-h/6} dx\, f(x) + \int_{-h/6}^{+h/2} dx\, f(x)$$

by taking linear combinations to cancel the h^4 correction terms

$$\int_{-h/2}^{+h/2} dx\, f(x) \cong \frac{81\left\{I^{(a)} + I^{(b)}\right\}-17I^{(0)}}{64}$$

The advantage of this scheme is that only four function evaluations are needed to perform an embedded error estimate, and all function evaluations are re-used at the next level of panel sub-division, with only two evaluations needed per each bifurcated panel at the next level of error testing. This scheme asymmetrically places the evaluation points and panel subdivisions, but of course the mirror symmetric analogue is readily available. Being a semi-open formula (no function evaluation is required on one of the panel boundaries) allows one to avoid problematic points in the energy spectrum (such as the origin).

Note that this scheme also comes at the cost of requiring a *negative* weight. This is actually an advantage for certain applications (such as ours) with positive definite integrands, as it provides another check on the adequacy of the interval decimation.

5. Catching Narrow resonances

Any automatic quadrature scheme admits the possibility that sub-grid scale features, such as very large but narrow resonances that fall between evaluation points, will fool the error estimate into a state of false convergence. (See Figure 7). Any guards against this possibility must come from supplementary information particular to the underlying system modeled, in our case the origin and behaviour of continuum state resonances[18].

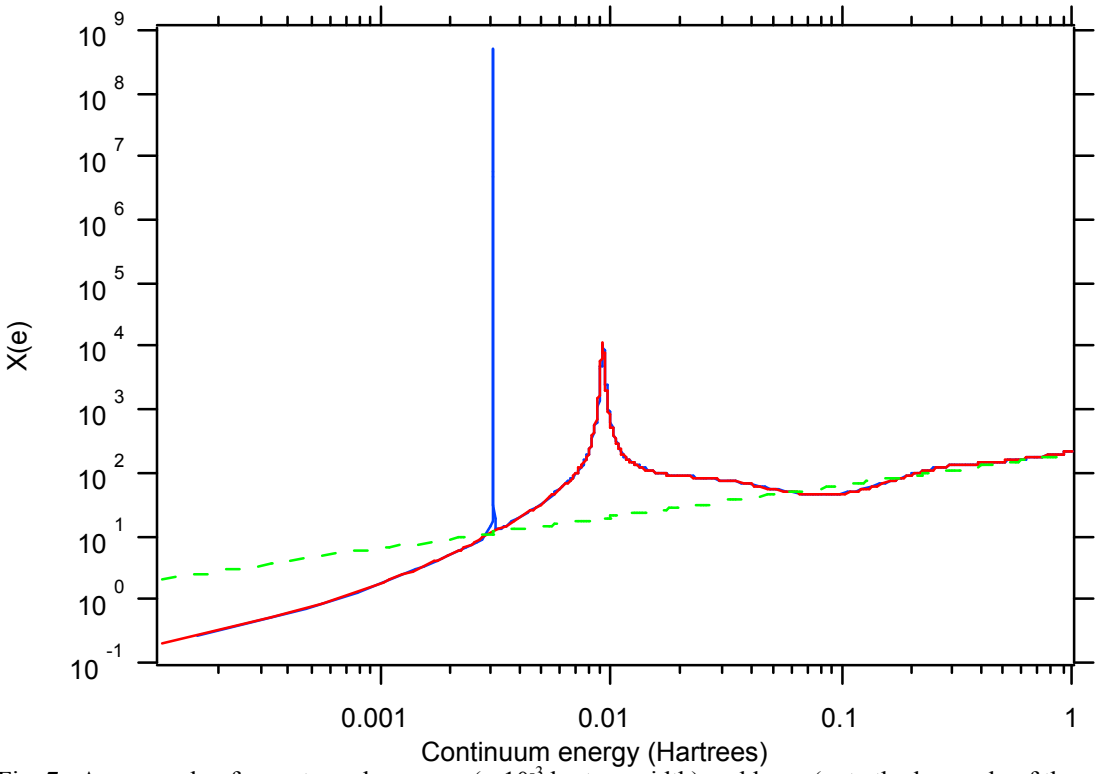

Fig. 7. An example of an extremely narrow (< 10^{-3} hartree width) and large (note the log scale of the y-axis) f7/2 orbital resonance for Uranium at 500eV and 1.9g/cc. Such features can occur on sub-grid size scales for automatic decimation integration schemes and be missed, yet they can contain a significant number (~0.1) of electrons. The dashed line represents ideal wave results.

The resonant properties of the continuum charge inside an ion sphere can be elucidated by writing

$$X \equiv \int_0^R dr \left\{P^2(r) + Q^2(r)\right\} = \frac{\Omega_<}{\pi \Gamma}$$

(for a given κ, index suppressed) where

$$\Omega_< \equiv \int_0^R dr \left\{a^2(r) + b^2(r)\right\}$$

$$a \equiv \frac{P_<(R)}{\sqrt{P_<^2(R) + \frac{1}{\alpha^2} Q_<^2(R)}} \qquad b \equiv \frac{\frac{1}{\alpha} Q_<(R)}{\sqrt{P_<^2(R) + \frac{1}{\alpha^2} Q_<^2(R)}} \qquad a^2 + b^2 = 1$$

Ω(ε), a(ε) and b(ε) are defined to be invariant to the normalization of the wave interior to the ion sphere and to be positive definite everywhere. (Note that we weigh the minor component by the fine structure constant so that it is of comparable magnitude to the major component. With such an appropriate scale factor the minor component may be simply related to the slope of the non-relativistic wave.) The denominator function is then exactly given as

$$\Gamma \equiv \frac{1}{\pi} \frac{S^2 + C^2}{P_<^2(R) + \frac{1}{\alpha^2} Q_<^2(R)} = \frac{\varepsilon}{p} \frac{1}{A_l^2} a^2 + \frac{p}{\varepsilon} A_l^2 \, \Theta^2 \qquad \Theta \equiv s_\kappa b + a \frac{\varepsilon}{p} \frac{\sqrt{A_l^2 A_{\tilde{l}}^2 - 1}}{A_l^2}$$

To obtain this simple form for Γ we employed two identities:

$$A_l^2(x) = j_l^2(x) + \eta_l^2(x) \qquad x \equiv pR$$

and the lesser known Bessel function identity

$$\left\{j_l(x) j_{\tilde{l}}(x) + \eta_l(x) \eta_{\tilde{l}}(x)\right\} = \sqrt{A_l^2(x) A_{\tilde{l}}^2(x) - 1}$$

This form for the denominator function is convenient in that the smooth Bessel amplitude function is an *analytic* polynomial[19] in $1/x^2$

$$A_l^2(x) = \sum_{m=0}^{l} c_m \frac{1}{x^{2m}} \qquad c_m \equiv \frac{(l+m)!}{(l-m)!}\frac{(2m-1)!!}{(2m)!!}$$

$$c_0 \equiv 1 \quad c_l = \left[(2l-1)!!\right]^2 \quad c_{l-1} = (2l-1)\left[(2l-3)!!\right]^2$$

This form also immediately shows that Γis positive definite, and to a very close approximation a sharp narrow minimum of Γoccurs near the zero of Θ. Careful inspection shows, due to the divergent behavior of A_l^2 for small arguments, that the closer this zero appears to the energy origin, the narrower is the dip in Γ and the smaller is its minimum value. These represent resonance features in the continuum density of states even when the interior wave solutions (the numerator Ω) show little variation.

In such circumstances we have approximately (dot denotes derivative with respect to energy)

$$\frac{1}{\Gamma} \approx \frac{1}{\Gamma_{\min} + \ddot{\Gamma}_{\min}\frac{1}{2}(\varepsilon - \varepsilon_{\min})^2}$$

and the charge under the resonance is

$$X \cong \frac{\Omega_<(\varepsilon_{\min})}{\pi}\int_{-\infty}^{\infty} d\varepsilon \frac{1}{\Gamma_{\min} + \ddot{\Gamma}_{\min}\frac{1}{2}(\varepsilon - \varepsilon_{\min})^2} = \frac{\Omega_<(\varepsilon_{\min})}{\sqrt{\Gamma_{\min}\ddot{\Gamma}_{\min}/2}}$$

Calculating the right hand side must be handled with care, as when resonances appear near the energy origin Γ is a vanishing small number

$$\Gamma_{\min} \cong \frac{e}{p}\frac{1}{A_l^2}a^2\Big|_{\varepsilon=\varepsilon_{\min}} \approx \varepsilon_{\min}^{l+1/2} << 1$$

whereas the second energy derivative (for L>0) diverges

$$\ddot{\Gamma}_{\min} \cong \left(\frac{p}{e}A_l^2\Big|_{\varepsilon_{\min}}\right)2\left(\frac{d\Theta}{d\varepsilon}\Big|_{\varepsilon_{\min}}\right)^2 \approx \frac{1}{\varepsilon_{\min}^{l+1/2}} >> 1$$

however, in such a way as their product is finite

$$X \cong \frac{\Omega_<(\varepsilon_{\min})}{\left|a\dot{\Theta}\right|_{\varepsilon_{\min}}}$$

(Note that for S waves the leading term of the second derivative has a different form which results in a vanishing strength under the resonance as it appears closer to the continuum threshold.) From this formula it is easy to demonstrate for arbitrary potentials

the continuity of X as conditions dissolve a bound state into the continuum (See Appendix 4).

Our strategy then is to perform an automatic decimation of the continuum energy grid using two convergence criteria. The first is the usual internal embedded estimator for the error inherent in each panel quadrature. But, additionally, we use the same function evaluation points to interpolate a(ε) and b(ε) in each angular momentum channel. This allows us to analytically determine the existence and then location of a zero of Θ(ε) within a panel. We may then optionally decimate the original panel by carving out a new panel in the interior, but only if a narrow resonance exists with a significant area relative to the original error estimate.

It is important to note (see Figure 8) that narrow resonances have been observed even in very high (L>20) angular channels for low density conditions of heavier elements.

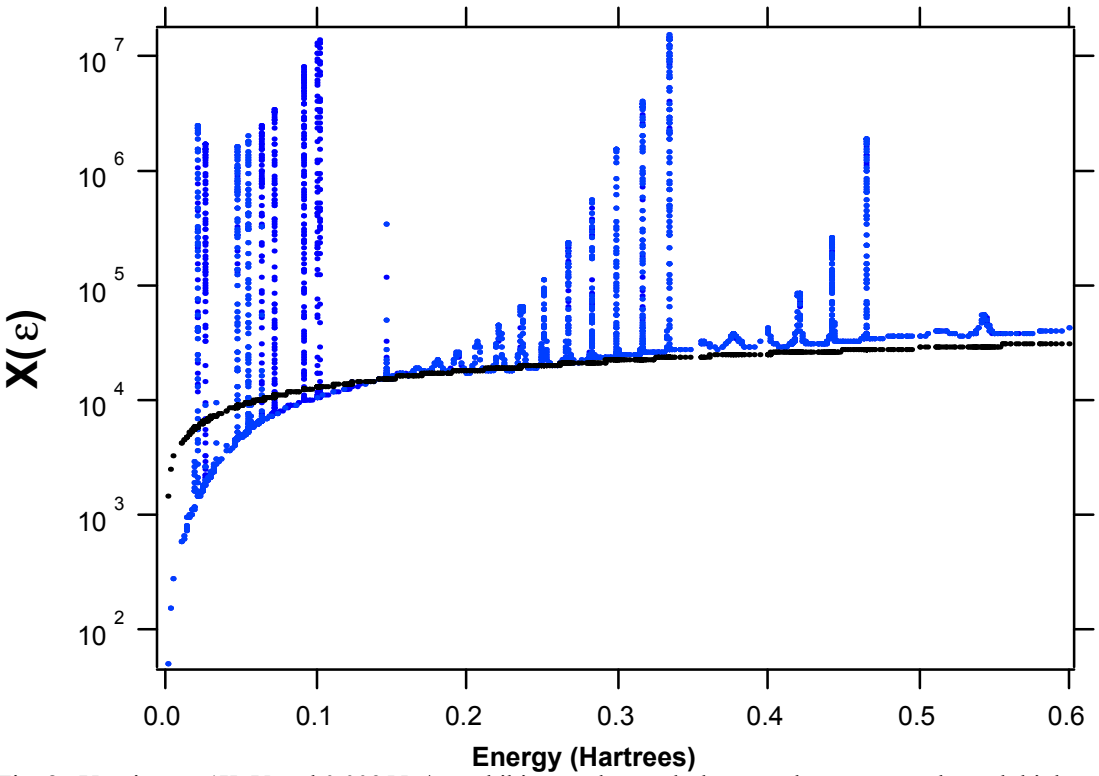

Fig. 8. Uranium at 1KeV and 0.00955g/cc exhibits nearly regularly spaced resonances through high angular momentum channels. The smooth curve represents ideal wave results.

5. Prototypical Results

The Purgatorio code has been run over a broad range of temperatures and densities and is being used to compare with other computational models and experimental results. Figures 9 and 10 illustrate typical comparisons of Hugoniot curves with the QEOS model[20]. Two qualitative observations can generally be made of our quantum model. First, atomic shell structure gives higher compression and Hugoniot structure that

Thomas-Fermi models cannot represent. Second, one sees that the Hugoniot correctly goes to the relativistic limit of seven times the initial density at high pressure (instead of $4\rho_0$ for Thomas-Fermi).

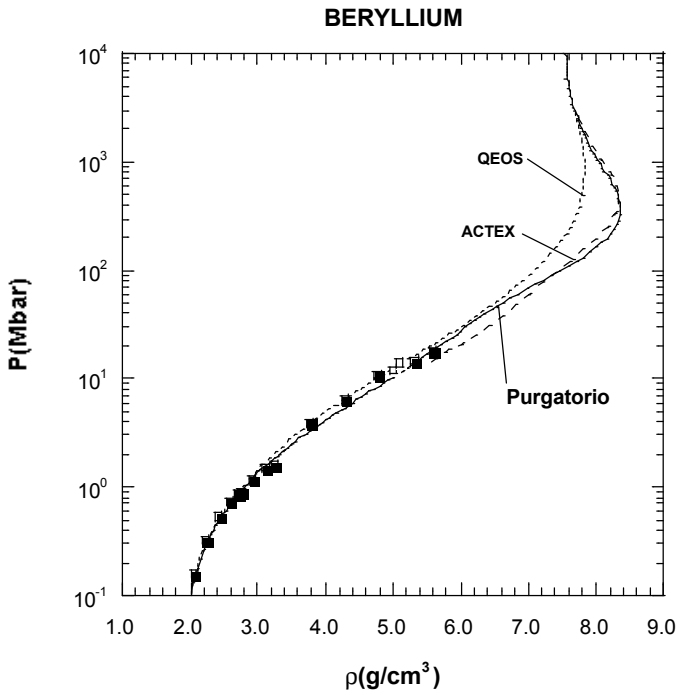

Fig. 9. A comparison of the principal Hugoniot for Be with Thomas-Fermi based QEOS and the strong coupling plasma quantum model of ACTEX[21].

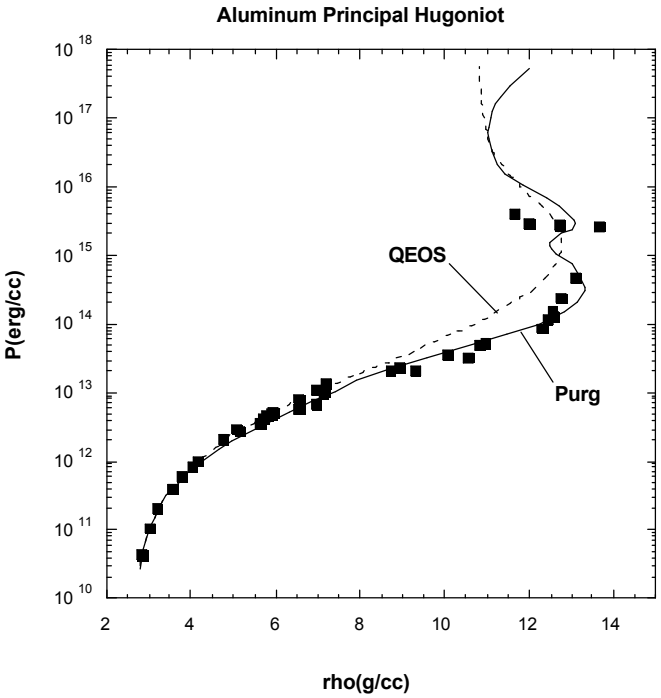

Fig. 10. Aluminum Hugoniot results, exemplifying shell structure and high pressure relativistic effects. Squares denote experimental results cited in the text.

Quantitative comparisons with experimental data[22] are limited by the paucity of accurate data in regimes where differences from semi-classical models are manifest. Comparisons performed so far have shown some improvement over QEOS results but still exhibit differences in lower density isochores (see Figure 11).

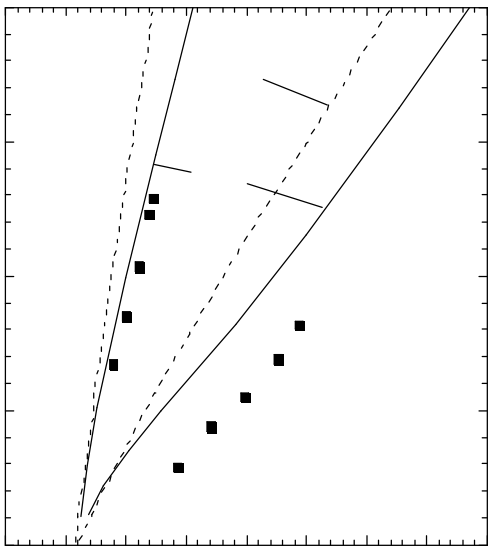

Fig. 11. Comparisons along aluminum isochoric data

6. Discussion

The emphasis of this paper has been on algorithms for the robust computation of EOS data. The objective of removing the main numerical approximations found in Inferno has been met, and data can now be automatically generated over a wider range of temperatures and densities. The main innovation of this work has been in the implementation of a novel scheme for automatic integration coupled with a semi-analytic method for catching narrow continuum resonances.

Model and algorithm development can be pursued in several avenues. The current algorithm is being augmented to routinely output electrical conductivity values[23] [24] [25]. We are undertaking a sensitivity study of our results to modifications in the local-density exchange-correlation functional presently employed. We also wish to explore the effects of going beyond (a) the jellium approximation[26] [27], and (b) fictitious 'average' ions in the plasma environment[28].

6. Acknowledgements

We wish to thank Walter Johnson for his contributions to the source code, and Richard Lee for his continued interest in this work. This work was performed under the auspices of the U.S. Department of Energy by University of California, Lawrence Livermore National Laboratory under Contract W-7405-Eng-48.

Appendices

A.1 Radial Dirac Conventions

The radial Dirac Hamiltonian, in spatial Bohr units and Hartee energy units, employs the sign and phase convention found in [29].

major: $$\frac{d}{dr}P+\frac{\kappa}{r}P=-\alpha\left(\frac{2}{\alpha^2}+\varepsilon-V\right)Q \qquad V\cong-\frac{Z}{r}$$

minor: $$\frac{d}{dr}Q-\frac{\kappa}{r}Q=+\alpha(\varepsilon-V)P$$

where we have

$$\kappa=-(l+1)\quad j=l+1/2\quad \tilde{l}=l+1\quad s_\kappa=-1$$
$$\kappa=l\quad j=l-1/2\quad \tilde{l}=l-1\quad s_\kappa=+1$$
$$\kappa(\kappa+1)=l(l+1)$$

Outside the ion sphere: $r>R\quad V=0$ waves obey

$$Q=-\frac{\alpha}{2+\alpha^2\varepsilon}\left\{\frac{d}{dr}P+\frac{\kappa}{r}P\right\}$$

$$\frac{d^2}{dr^2}P+\left\{\varepsilon\left(2+\alpha^2\varepsilon\right)-\frac{l(l+1)}{r^2}\right\}P=0$$

For positive energy define $p^2\equiv\varepsilon\left(2+\alpha^2\varepsilon\right)$; we have the explicit solution

$$\begin{Bmatrix}P\\Q\end{Bmatrix}=\sqrt{\frac{p}{\pi\varepsilon}}\begin{Bmatrix}j_l(pr)\cos\Delta-\eta_l(pr)\sin\Delta\\-s_\kappa\dfrac{\alpha\varepsilon}{p}\quad\left(j_{\tilde{l}}(pr)\cos\Delta-\eta_{\tilde{l}}(pr)\sin\Delta\right)\end{Bmatrix}$$

The first few spherical Bessel functions are explicitly

$$j_0(x)=\sin(x)\qquad \eta_0(x)=-\cos(x)$$
$$j_1(x)=-\cos(x)+\frac{\sin(x)}{x}\qquad \eta_1(x)=-\sin(x)-\frac{\cos(x)}{x}$$

and we have also utilized the spherical Bessel identities (valid for regular and irregular spherical Bessel functions) to obtain the minor component waves

$$\frac{d}{dx}z_l(x)+\frac{l}{x}z_l(x)-z_{l-1}(x)=0$$
$$\frac{d}{dx}z_l(x)-\frac{l+1}{x}z_l(x)+z_{l+1}(x)=0$$

The ideal continuum waves are normalized such that

$$\int_0^\infty dr\,\{P_\varepsilon P_{\varepsilon'}+Q_\varepsilon Q_{\varepsilon'}\}=\delta(\varepsilon-\varepsilon')$$

by using the identity

$$\int_{-\infty}^{\infty} dr\,\sin(pr)\sin(p'r)=\frac{\pi}{2}\delta(p-p')=\frac{\pi}{2}\frac{p}{1+\alpha^2\varepsilon}\delta(\varepsilon-\varepsilon')$$

Inside the ion sphere the wave is

$$\begin{Bmatrix}P\\Q\end{Bmatrix}=A\begin{Bmatrix}P_<(r)\\Q_<(r)\end{Bmatrix}$$

where $P_<$ and $Q_<$ are arbitrary un-normalized solutions to Dirac's equation and A is a normalization constant. Matching major and minor components at the ion sphere radius we may solve for the two unknowns Δ and A. The result is that the phase is given by

$$\tan\Delta=\frac{S}{C}$$

where

$$S\equiv s_\kappa\sqrt{\frac{\varepsilon\pi}{p}}P_<(R)j_{\tilde{l}}(pR)+\sqrt{\frac{\pi p}{\varepsilon}}\frac{1}{\alpha}Q_<(R)j_l(pR)$$
$$C\equiv s_\kappa\sqrt{\frac{\varepsilon\pi}{p}}P_<(R)\eta_{\tilde{l}}(pR)+\sqrt{\frac{\pi p}{\varepsilon}}\frac{1}{\alpha}Q_<(R)\eta_l(pR)$$

While the amplitude is

$$A=\frac{1}{\sqrt{S^2+C^2}}$$

This result additionally required the ansatz

$$\sin\Delta = \frac{S}{\sqrt{S^2 + C^2}} \qquad \cos\Delta = \frac{C}{\sqrt{S^2 + C^2}}$$

and employed the identity

$$s_\kappa \{ j_l \eta_{\tilde{l}} - \eta_l j_{\tilde{l}} \} = 1$$

which is a consequence of the Wronskian

$$j_l(x)\left\{\frac{d}{dx}\eta_l(x)\right\} - \left\{\frac{d}{dx} j_l(x)\right\}\eta_l(x) = 1$$

A.2 Useful radial integral identities

This identity

$$X \equiv \int_0^R dr \, \{P^2(r) + Q^2(r)\} = \frac{1}{\alpha}\left\{ Q\frac{dP}{d\varepsilon} - P\frac{dQ}{d\varepsilon}\right\}\Big|_R$$

can be derived as follows. Write the radial Dirac equation in matrix form:

$$\hat{h}_{Dirac}\begin{pmatrix} P_b \\ Q_b \end{pmatrix} = \left[-\underline{\underline{\partial}} - \underline{\underline{\kappa}} + \underline{\underline{\upsilon}} - \varepsilon_a \underline{\underline{\alpha}}\right]\begin{pmatrix} P_a \\ Q_a \end{pmatrix} \equiv$$
$$\left[-\begin{pmatrix} 0 & -\frac{d}{dr} \\ +\frac{d}{dr} & 0 \end{pmatrix} - \begin{pmatrix} 0 & \frac{\kappa}{r} \\ \frac{\kappa}{r} & 0 \end{pmatrix} + \begin{pmatrix} \alpha V & 0 \\ 0 & -\frac{1}{\alpha}\left(2 - \alpha^2 V\right) \end{pmatrix} - \begin{pmatrix} \alpha & 0 \\ 0 & \alpha \end{pmatrix}\varepsilon_a \right]\begin{pmatrix} P_a \\ Q_a \end{pmatrix} = 0$$

Then the energy derivatives of the waves satisfy the inhomogenous equation

$$\left[-\underline{\underline{\partial}} - \underline{\underline{\kappa}} + \underline{\underline{\upsilon}} - \varepsilon_a \underline{\underline{\alpha}}\right]\begin{pmatrix} f \\ g \end{pmatrix} \equiv \underline{\underline{\alpha}}\begin{pmatrix} P_b \\ Q_b \end{pmatrix} \qquad \begin{pmatrix} f \\ g \end{pmatrix} \equiv \begin{pmatrix} (P_a - P_b)/(\varepsilon_a - \varepsilon_b) \\ (Q_a - Q_b)/(\varepsilon_a - \varepsilon_b) \end{pmatrix} \Rightarrow \begin{pmatrix} dP/d\varepsilon \\ dQ/d\varepsilon \end{pmatrix}$$

leading to

$$(P_a \quad Q_a)\underline{\underline{\partial}}\begin{pmatrix} f \\ g \end{pmatrix} - (f \quad g)\underline{\underline{\partial}}\begin{pmatrix} P_a \\ Q_a \end{pmatrix} = -\alpha\left(P_a^2 + Q_a^2\right) \;\Rightarrow\; \left(P_a^2 + Q_a^2\right) = \frac{1}{\alpha}\frac{d}{dr}\{gP_a - fQ_a\}$$

upon which the integral of charge inside the ion sphere can be expressed in terms of end point values.

Similarly we can establish the identity

$$(\varepsilon_b - \varepsilon_a) M_{ab} = -W_{ab} \qquad M_{ab} = \int_0^{R_{ion}} dr \{P_a P_b + Q_a Q_b\}$$

where

$$W_{ab} \equiv -2 \int_0^{R_{ion}} dr \left\{ P_a \frac{dQ_b}{dr} - Q_a \frac{dP_b}{dr} \right\}$$

This is done directly from

$$(\varepsilon_b - \varepsilon_a) \int_0^{R_{ion}} dr \{P_a P_b + Q_a Q_b\} = \int_0^{R_{ion}} dr \, (P_a \; Q_a) \left\{ \hat{h}_{Dirac} \begin{pmatrix} P_b \\ Q_b \end{pmatrix} \right\} - \left\{ (P_a \; Q_a) \left(\hat{h}_{Dirac} \right)^T \right\} \begin{pmatrix} P_b \\ Q_b \end{pmatrix}$$

$$= -2 \int_0^{R_{ion}} dr \, (P_a \; Q_a) \partial \begin{pmatrix} P_b \\ Q_b \end{pmatrix}$$

By the symmetry of M_{ab} with respect to interchange of indices {a,b} we have $-W_{ab} = W_{ba}$. Using this fact and integrating W_{ab} by parts one obtains

$$W_{ab} = -(P_a Q_b - Q_a P_b) \Big|^{R_{ion}}$$

A.3 Identities for partial wave summation accelerations

It is useful to accelerate partial wave evaluations by subtracting the ideal (zero potential) wave contribution for each angular channel from that of the distorted wave value, truncating the summation when this difference becomes negligible. The contributions from all higher channels are then included in approximate fashion by adding a closed form expression for the ideal contribution from all channels. In this appendix we provide formulas used to accelerate sums over

$$X_\kappa(\varepsilon) \equiv \int_0^R dr \left\{ P_\kappa^2(r) + Q_\kappa^2(r) \right\} = \frac{1}{\alpha} \left\{ Q_\kappa \frac{dP_\kappa}{d\varepsilon} - P_\kappa \frac{dQ_\kappa}{d\varepsilon} \right\} \Big|_R$$

Using the first equality and expressions for the ideal waves from Appendix 1 we obtain

$$X(\varepsilon) = \sum_\kappa 2|\kappa| X_\kappa(\varepsilon) = \int_0^{R_{ion}} dr \, \frac{2p}{\pi\varepsilon} \sum_\kappa |\kappa| j_l^2(pr) + \frac{2\alpha\varepsilon}{\pi p} \sum_\kappa |\kappa| j_{\tilde{l}}^2(pr)$$

$$= \frac{(1 + \alpha^2 \varepsilon)}{\pi^2 p} p^2 \left\{ \frac{4}{3} \pi R_{ion}^3 \right\}$$

by using the identity

$$\sum_{\kappa=\pm1}^{\pm\infty}|\kappa|j_l^2(x)=\sum_{\kappa=\pm1}^{\pm\infty}|\kappa|j_{\tilde{l}}^2(x)=\sum_{l=0}^{\infty}(2l+1)j_l^2(x)=x^2$$

Using the second form for X_κ we obtain

$$X_\kappa(\varepsilon)=X_\kappa^{(0)}(\varepsilon)+X_\kappa^{(1)}(\varepsilon)$$

$$X_\kappa^{(0)}=-\frac{s_\kappa}{\pi}j_l(pr)j_{\tilde{l}}(pr)\left\{\sqrt{\frac{p}{\varepsilon}}\frac{d}{d\varepsilon}\sqrt{\frac{\varepsilon}{p}}-\sqrt{\frac{\varepsilon}{p}}\frac{d}{d\varepsilon}\sqrt{\frac{p}{\varepsilon}}\right\}=-\frac{s_\kappa}{\pi p^2}j_l(pr)j_{\tilde{l}}(pr)$$

$$X_\kappa^{(1)}=\left\{\frac{1}{\pi}r\frac{dp}{d\varepsilon}\right\}\left\{-s_\kappa\left(j_l\frac{d}{dpr}j_{\tilde{l}}-j_{\tilde{l}}\frac{d}{dpr}j_l\right)\right\}=\left\{\frac{(1+\alpha^2\varepsilon)}{\pi p}r\right\}\left\{j_l^2+j_{\tilde{l}}^2-\frac{2|\kappa|}{pr}j_lj_{\tilde{l}}\right\}$$

The association with the analytic form for X(ε) is provided by

$$\sum_\kappa 2|\kappa|X_\kappa^{(0)}=0$$

the aforementioned Bessel summation identity and the less well known identity[30]

$$\sum_{m=1}^{\infty}m^2j_m(x)j_{m-1}(x)=\frac{1}{3}x^3$$

A.4 Continuity of states dissolving into the continuum

We now proceed to demonstrate that the value of X is continuous as a bound state dissolves into the continuum. First, let us consider the value of X when a state is just barely bound. Matching interior and exterior solutions (here A and B are normalization constants)

$$A\begin{Bmatrix}P_<(R)\\Q_<(R)\end{Bmatrix}=B\begin{Bmatrix}P_>(R)\\Q_>(R)\end{Bmatrix}$$

we use, outside the ion-sphere where V=0

$$\begin{Bmatrix}P_>(r)\\Q_>(r)\end{Bmatrix}\equiv\begin{Bmatrix}\lambda^l h_l(\lambda r)\\-s_\kappa\dfrac{\alpha\lambda}{2+\alpha^2\lambda}\lambda^l h_{\tilde{l}}(\lambda r)\end{Bmatrix}\xrightarrow[\varepsilon\to0]{}\begin{Bmatrix}1/r^l\\-\dfrac{\alpha}{2}(\kappa-l)\dfrac{1}{r^{l+1}}\end{Bmatrix}$$

For negative energies we defined $-\lambda^2 \equiv \varepsilon\left(2+\alpha^2\varepsilon\right)$ and the first few Hankel functions were introduced as

$$h_0(x)=e^{-x} \qquad h_1(x)=\left(1+x^{-1}\right)e^{-x} \qquad h_2(x)=\left(1+3x^{-1}+3x^{-2}\right)e^{-x}$$
$$h_l(x)=e^{-x}\sum_{m=0}^{l}(2x)^{-m}\frac{(l+m)!}{m!(l-m)!}$$

One finds

$$X_{\varepsilon\to 0-}=\frac{A^2\int_0^R dr\left\{P_<^2+Q_<^2\right\}}{A^2\int_0^R dr\left\{P_<^2+Q_<^2\right\}+B^2\int_R^\infty dr\left\{P_>^2+Q_>^2\right\}}=\frac{\Omega_<}{\Omega_<+a^2\left\{\dfrac{\int_R^\infty dr\left\{P_>^2+Q_>^2\right\}}{P_>^2(R)}\right\}}$$

Our proof therefore consists of establishing the correspondence

$$\Omega_<+a^2\left\{\frac{\int_R^\infty dr\left\{P_>^2+Q_>^2\right\}}{P_>^2(R)}\right\} \quad \Leftrightarrow \left|a\dot{\Theta}\right|$$

For the left hand side we have

$$\frac{\int_R^\infty dr\left\{P_>^2+Q_>^2\right\}}{P_>^2(R)}=\frac{R}{2l-1}+\frac{\alpha^2}{4}\frac{(\kappa-l)^2}{2l+1}\frac{1}{R} \qquad l>0$$
$$=\infty \qquad l=0$$

and use

$$\Omega_< = a\dot{b}-b\dot{a}$$

which is a restatement of the identity of Appendix 2, for arbitrary normalization.

For the right hand side it is now a simple arithmetic to show for $j=l+1/2$ that

$$\Theta=-b+a\frac{\varepsilon}{p}\left\{\frac{2l+1}{x}-\frac{x}{2l-1}+O\left[x^3\right]\right\}$$

$$\Theta = 0 \quad \Rightarrow \quad b \cong a\left\{\frac{2l+1}{R}\frac{1}{2+\alpha^2\varepsilon} - \frac{\varepsilon R}{2l-1} + \ldots\right\}$$

$$\Theta = -b + a\left\{\frac{b}{a}\right\} - a\left\{\frac{2l+1}{R}\frac{\alpha^2}{4} + \frac{R}{2l-1} + \ldots\right\}$$

while for $j = l - 1/2$

$$\Theta = b + a\frac{\varepsilon}{p}\left\{\frac{x}{2l-1} + O\left[x^3\right]\right\}$$

$$\Theta = 0 \quad \Rightarrow \quad b \cong -a\left\{\frac{\varepsilon R}{2l-1} + \ldots\right\}$$

$$\Theta = b + a\left\{-\frac{b}{a}\right\} + a\left\{\frac{R}{2l-1} + \ldots\right\}$$

completing the proof.

---

[1] Liberman DA. Self-consistent field model for condensed mater. Phys. Rev. B 1979;20:4981-4989

[2] Johnson WR. Atomic Physics: A Numerical Approach. www.nd.edu/~johnson/ 1999

[3] Goano M. Series expansion of the Fermi-Dirac Integral $F_j(x)$ over the entire domain of real j and x. Solid State Electronics 1993;36:217-221

[4] Gong Z, et al. Generalized Fermi-Dirac functions and derivatives: properties and evaluation. Comp. Physics Commun. 2001;136:294-309

[5] Segura J, Gil A. Elf and Gnome: Two tiny codes to evaluate the real zeros of the Bessel functions of the first kind for real orders. Comp. Phys. Commun. 1999;117:250-262

[6] Englert BG. Semiclassical Theory of Atoms. Lecture Notes in Physics 300. Springer-Verlag 1988.

[7] Bennett BI, Liberman DA. Inferno. Los Alamos National Laboratory Report 1985; LA-10309-M

[8] Liberman DA, Bennet BI. Atomic vibrations in a self-consistent-field atom-in-jellium model of condensed matter. Phys. Rev. B 1990;42:2475-2484

[9] Perez-Bernal F, et al. Continuum discretization using orthogonal polynomials. Phys. Rev. A 2003;67:052108

[10] Mayers DF, Turner DM. The evaluation of relativistic Oscillatory wavefunctions on a logarithmic grid. J. Comp. Phys. 1984;55:397-407

[11] Press WH, et al. Numerical Recipes, The art of Scientific Computing, 2nd ed. Cambridge 1992. p.727-735.

[12] Bar-Shalom A, et al. Phase-amplitude algorithms for atomic continuum orbitals and radial integrals. Comp. Phys. Commun. 1996;93:21-32

[13] Sidky E, Ben-Itzhak I. Phase-amplitude method for calculating resonance energies and widths for one-dimensional potentials. Phys. Rev. A 1999;60:3586-3592

[14] Robicheaux F, et al. Generalized WKB and Milne solutions to one-dimensional wave equations. Phys. Rev. A 1987;35:3619-3630
[15] Haug E. Simple equation of state for partially degenerate simirelativistic electrons. Astronomy and Astrophysics 2003;407:787-789
[16] Shlomo S, et al. Single particle level density in a finite depth potential well. Phys. Rev. C 1997;55:1972-1981
[17] Gander W, Gautschi W. Adaptive Quadrature-Revisited. BIT 2000;40:84-101
[18] More RM, Gerjuoy E. Properties of Resonance Wave Functions. Phys. Rev. A 1973;7:1288-1303
[19] Calogero F. Variable Phase approach to potential scattering. Academic Press, 1967
[20] More RM, et al. A new quotidian equation of state (QEOS) for hot dense matter. Phys. Fluids 1988;31:3059-3078
[21] Rogers F. Ionization equilibrium and equation of state in strongly coupled plasmas. Phys. Plasmas. 2000;7:51-58
[22] Renaudin P, et al. Combined Pressure and Electrical-Resistivity Measurements of Warm dense Aluminum and Titanium Plasmas. Phys. Rev. Lett. 2002;88:215001
[23] Rinker G. The electrical conductivity of an Arbitrarily Dense Plasma. Los Alamos National Laboratory Report 1984; LA-9872-MS
[24] Redmer R. Electrical conductivity of dense metal plasmas. Phys. Rev. E 1999;59:1073-1081
[25] Kuhlbrodt S, Redmer R. Transport coefficients for dense metal plasmas. Phys. Rev. E 2000;62:7191-7200
[26] Kiyokawa S. One-component plasmas with self-consistently determined core electrons. J. Phys. Soc. Japan 1995;64:4708-4725
[27] Ofer D, et al. Interionic correlations in plasmas: Thomas-Fermi hypernetted-chain density-functional theory. Phys. Rev. A 1988;38:5801-5809
[28] Pain JC, Blenski T. Self-consistent approach for the thermodynamics of ions in dense plasmas in the superconfiguration approximation. J.Q.S.R.T 2003;81:355-369
[29] Johnson WR. Free-Particle Continuum Density. www.nd.edu/~johnson/ 2003
[30] Watson GN. A Treatise on the theory of Bessel Functions. Cambridge, 1952